J. Nucl. Phys. Mat. Sci. Rad. A. Vol. 10, No. 1 (2022), pp.11–20

CHITKARA

Journal of Nuclear Physics, Material Sciences, Radiation and Applications
Journal homepage: https://jnp.chitkara.edu.in/

Iscovector Giant Dipole Resonance in ^{175}Lu within the Linear Response Theory

Abhishek*

Department of Physics, Indian Institute of Technology Roorkee, Roorkee 247 667, India

*abhishek@ph.iitr.ac.in (Corresponding Author)

ARTICLE INFORMATION

Date of Submission: October 28, 2022
Received: November 28, 2022
Accepted: November 23, 2022
Published Online: December 19, 2022

Keywords:
Giant Resonances, Nuclear Structure

DOI: 10.15415/jnp.2022.10103

ABSTRACT

Background: Isovector giant dipole resonance (IVGDR) is one of the hallmark probes in nuclear structure studies. Almost all the nuclei exhibit IVGDR in the nuclear chart. Most of our understanding of GDR comes from studying the GDR in even-even nuclei. Many theoretical works based on random phase approximation (RPA) have been carried out to understand GDR's physical nature, primarily in even-even nuclei. The experimental and theoretical search for these modes is very scarce in odd-mass deformed nuclei.

Purpose: We investigate the IVGDR in a well-deformed odd-even ^{175}Lu with two different GDR models, categorized as macroscopic and microscopic models. We compare the results obtained by two models with the available experimental data for the photo-absorption cross-section.

Methods: The microscopic approach for giant dipole resonance (GDR) is based on the linear response theoory which simulates the nuclear density response to the dipole radiation through single-particle wave functions. The wave functions are calculated with a triaxial Woods-Saxon (WS) potential. The nuclear shape is obtained using the same WS potential in a microscopic-macroscopic approach. The macroscopic approach models the GDR as the sum of the Lorentzians with peaks at resonance energies given by frequencies corresponding to the model Hamiltonian. The model Hamiltonian for the macroscopic model is the sum of the anisotropic harmonic oscillator Hamiltonian and a dipole-dipole interaction.

Results: The results for the photo-absorption cross-section obtained from both the models are compared with the experimental data reported in Ref. [1]. The value of the deformation parameter obtained from our microscopic-macroscopic approach is compared with the experimentally obtained value of deformation as well as with the results of the finite-range droplet mode (FRDM).

Conclusion: The value of the deformation parameter (β_2) obtained from our model for PES lies between the result of FRDM and the experimental β_2. The results from the microscopic model show a splitting of GDR strength into K = 0 and K = 1 components due to large quadrupole deformation. The splitting of the GDR peak is consistent with the experimental data. The microscopic approach performs better overall, but in the lower energy region (8-13 MeV), the results obtained from the macroscopic model perform better.

1. Introduction

The atomic nucleus is a fnite-size quantum many-body system that exhibits collective excitations connected to the underlying nuclear structure. One of the most common examples of such collective excitations is the Giant resonances (GRs) [2]. GRs are an efective probe into the response of a nucleus subjected to a weak electromagnetic external perturbation. Quantum mechanically, it is the transition between the ground state and a collective excited state. Isovector E_1 (dipole) transition has the highest probability, and thus giant dipole resonance (GDR), which primarily refers to isovector GDR, is the most prominent among all the GRs. Since its discovery in 1937 [3], there has been an extensive study in the feld of GDR, both experimentally [4, 5, 6, 7, 8] and theoretically [9, 10, 11, 12, 13, 14, 15].

Theoretical models can be broadly identifed as either macroscopic or microscopic. Macroscopic models [11, 16, 17] calculate the GDR observable by connecting the GDR to the deformation parameters describing the nuclear shape. Macroscopic models have successfully reproduced overall GDR observ-ables even at fnite temperature and spin [8, 10]. Macroscopic models connect the GDR directly to the underlying nuclear shape and model the GDR as the out-of-phase oscillations between the proton and neutron fuids under the infuence of an external electromagnetic feld

ISSN No.: 2321-8649(Print) ISSN No.: 2321-9289(Online); Registration No. : CHAENG/2013/51628

which can be induced by an emitted or absorbed photon. Coupling of GDR directly to the shape of the nucleus provides useful structure information in the macroscopic approaches. In a spherical nucleus, the GDR strength manifests as a single peak, but in a deformed nucleus, it splits depending upon the shape of the nucleus [2, 18]. In a prolate nucleus, the GDR strength splits into two components because the frequency of GDR oscillation is inversely proportional to the length of the semi-major axis. One component represents the oscillation along the symmetry axis ($K = 0$), and the other component is along the perpendicular plane to the symmetry axis ($K = 1$). The $K = 1$ component is always doubly degenerate for a prolate shape as it represents the oscillations along two shorter semi-major axes, which are equal in length.

On the other hand, the microscopic models model the GDR as the superposition of particle-particle (*pp*), particle-hole (*ph*), and hole-hole (*hh*) excitations. There are several microscopic models which are developed over the years, such as the phonon damping model (PDM) [19], the time dependant Hartree-Fock (TDHF) [15], the separable random-phase approximation (SRPA) [20], the extended quantum molecular dynamics (EQMD) model [21], the fnite amplitude quasiparticle random phase approximation (FAM-QRPA) [22], the QRPA based on the relativistic Hartree-Bogoliubov model [23], and the relativistic random phase approximation (RRPA) [24]. There are stochastic [25], and semi-classical [26] approaches as well. Linear response theory (LRT) framework [27, 28, 29] is one of the most common RPA-based microscopic methods which addresses the collective excitations in the nucleus. Many of the theoretical works primarily focus on the even-even nuclei, and almost all our understanding of GDR comes from studying the even-even nuclei. The experimental and theoretical studies which are focused on odd-even nuclei are scarce.

One of such odd-even nuclei is the ^{175}Lu where the experimental data is available for a long time [1], but there have been only a few theoretical works have been carried out for this nucleus. The astrophysical importance [30] of this nucleus necessitates more investigation with more microscopic approaches. Recent work [31] in this nucleus has been successful in explaining the GDR features in the lower energy and uses Translation and Galilean quasiparticle phonon nuclear model (TGI-QPNM) [32]. The TGI-QPNM is based on the one-phonon QRPA method, in which only the harmonic efects are taken into account [31]. In this study, the shape of the nucleus is taken as the input parameter and is inferred from the empirical fndings on the other hand, in this work, we discuss a microscopic approach for GDR in deformed nuclei within the framework of linear response theory (LRT) [33] that can be combined with a microscopic-macroscopic approach for nuclear potential energy calculations. The equilibrium deformation of the nucleus is identifed by minimizing the potential energy in deformation space calculated using the Strutinsky method with the triaxial Woods-Saxon (WS) potential. The single-particle wavefunctions resulting from the same calculations are utilized to evaluate the GDR properties. We compare the macroscopic and microscopic approaches to GDR by comparing the results with the experimental data reported in Ref. [1].

The present article is organized as follows: the theoretical formalism for the nuclear potential energy surface (PES) calculations and the WS mean-feld, along with the formalism of macroscopic and microscopic model for GDR, is discussed in section 2. In section 3, we present our results, and the conclusions are given in the section 4.

2. Theoretical Framework

The GDR is built on a nuclear state and hence the methods to calculate the structure of the state and the collective excitation can be better described in parts. We start with the description of our mean-feld calculations and subsequently present the details of the shell correction method, microscopic and macroscopic approaches for GDR, and the wavelet analysis of GDR cross-sections.

2.1. The Triaxial Woods-Saxon Potential

In a phenomenological way, the nuclear potential is considered as a sum of central mean-feld-potential $V_{ws}(\vec{r},\,\theta,\,\phi)$, the Coulomb potential $V_{coul}(\vec{r},\,\theta,\,\phi)$ and the spin-orbit potential $V_{s.o.}(\vec{r},\,\theta,\,\phi)$, given by

$$V(\vec{r},\,\theta,\,\phi) = V_{ws}(\vec{r},\,\theta,\,\phi) + V_{coul}(\vec{r},\,\theta,\,\phi) + V_{s.o.}(\vec{r},\,\theta,\,\phi) \tag{1}$$

2.1.1. Central Mean-Field Potential The central mean-field potential is described by the Woods-Saxon form

$$V_{ws}(\vec{r},\,\theta,\,\phi) = -\frac{V_0\left[\kappa\left(\dfrac{N-Z}{N+Z}\right)\right]}{1+\exp\left\{\dfrac{\mathrm{dist}\left[\vec{r}(\theta,\,\phi),\,\vec{r}_s(\theta_s,\,\phi_s)\right]}{b}\right\}} \tag{2}$$

where V_0 is the depth of potential, $\mathrm{dist}\left[\vec{r}(\theta,\,\phi),\,\vec{r}_s(\theta_s,\,\phi_s)\right]$ is the distance between a point $r(\theta,\,\phi)$ and the nearest point $r_s(\theta_s,\,\phi_s)$ on the nuclear surface, b represents the surface thickness of the potential, + and − signs stand for protons and neutrons, respectively. K represents the strength of the isospin dependence.

The surface $R(\theta,\,\phi)$ of a deformed nucleus can be written as

$$R(\theta,\ \phi) = CR_0\left[\sum_{\lambda=0}^{\lambda_{\max}}\sum_{\mu=-\lambda}^{\lambda} a_{\lambda\mu}Y_{\lambda\mu}(\theta,\ \phi)\right] \tag{3}$$

where R_0 is the radius of the equivalent spherical nucleus with the same volume, $a_{\lambda\mu}$ are deformation parameters, $Y_{\lambda\mu}$ are the spherical harmonics, and C is the volume conservation constant. Restricting to only even and lowest multipoles up to $\lambda = 4$, $R(\theta, \phi)$ can be written as

$$\begin{aligned} R(\theta,\ \phi) = CR_0\big[&a_{00}Y_{00} + a_{20}Y_{20} + a_{22}\left(Y_{22} + Y_{2-2}\right) \\ &+ a_{40}Y_{40} + a_{42}\left(Y_{42} + Y_{4-2}\right) + \\ &a_{44}\left(Y_{44} + Y_{4-4}\right)\big]. \end{aligned} \tag{4}$$

The parameters $a_{\lambda\mu}$ can be defined in terms of deformation parameters β, β_4, γ as

$$\begin{aligned} a_{00} &= \sqrt{4\pi}, \\ a_{20} &= \beta_2\cos(\gamma) \\ a_{22} &= a_{2-2} = \frac{\beta_2}{\sqrt{2}}\sin(\gamma) \\ a_{40} &= \frac{1}{6}\left[5\cos^2(\gamma)+1\right]\beta_4, \\ a_{42} &= a_{4-2} = -\frac{1}{12}\sqrt{30}\sin(2\gamma)\beta_4, \text{ and} \\ a_{44} &= \frac{1}{12}\sqrt{70}\sin^2(\gamma)\beta_4. \end{aligned} \tag{5}$$

2.1.2. Coulomb Potential The Coulomb term is given by

$$V_{coul}(\vec{r},\ \theta,\ \phi) = e\int_v \frac{\rho(\vec{r}')}{\left|\vec{r}-\vec{r}'\right|}d\vec{r}', \tag{6}$$

where $\rho(\vec{r}') \equiv \rho_0(Z-1)e/V$, represents the nuclear charge density with uniform charge distribution. Here e and V represent the electronic charge and the volume of the nucleus, respectively. This can be expressed in terms of multipole expansion through spherical harmonics as

$$V_{coul}(\vec{r},\ \theta,\phi) = \sum_{\lambda\Sigma} V^c_{\lambda\Sigma}(r)Y_{\lambda\Sigma}(\theta,\ \phi). \tag{7}$$

2.1.3. Spin-Orbit Potential The spin-orbit potential is given by

$$V_{s.o.}(\vec{r},\ \theta,\ \phi) = V_2(\vec{r},\ \theta,\ \phi)\vec{\sigma}\cdot\vec{\ell},$$

where

$$\begin{aligned} V_2(\vec{r},\ \theta,\ \phi) &\propto \frac{1}{r}\frac{dV_1(\vec{r},\ \theta,\ \phi)}{dr}, \\ &= -\frac{\lambda_{s.o}\hbar^2}{4M^2c^2}\frac{1}{r}\frac{dV_1(\vec{r},\ \theta,\ \phi)}{dr}. \end{aligned} \tag{8}$$

Here $V_1(r, \theta, \phi)$ has the Woods-Saxon form (2). $\lambda_{s.o}$, $\vec{\sigma}$, $\vec{\ell}$ and M represent the spin-orbit potential strength parameter, Pauli matrices, angular momentum operator and the mass of the nucleon, respectively.

We construct the Hamiltonian matrix in a harmonic oscillator basis with quantum numbers n (radial quantum number), ℓ (orbital quantum number), j (total angular momentum quantum number) and Ω (quantum number for the projection of j on the third axis). The basis is set up for defned maximum values of n and j. These values are crucial, as discussed in Sec. 2.2. The radial part of basis wave functions is evaluated up to 30 fm in steps of 0.1 fm. The parameters for Woods-Saxon potential were chosen from the universal parameter set [34]. The Hamiltonian is then diagonalized numerically to obtain the single-particle energies (ε_i) and the corresponding eigenvectors *(D^i)* separately for protons and neutrons. The single particle wave functions are of the form

$$\psi^i \sum_{n,\ \ell,\ j,\ \Omega} D^i_{n\ell j\Omega}R_{n\ell}(r)\times\left[Y_{\ell m}(\theta,\ \phi)\otimes\chi_{\frac{1}{2}}\right]^{\Omega}_{j}, \tag{9}$$

where $R_{n\ell}$ and $\chi_{\frac{1}{2}}$ represent the radial wave function and the wave function corresponding to the spin of nucleons, respectively.

2.2. Shell Corrections

The total free energy of the nucleus can be defned as the sum of the smooth liquid drop model (LDM) energy and the oscillatory part representing the strength of the quantum efects [35, 36], which can be written as

$$E_{TOT} = E_{LDM} + \sum_{Z,\ N}\delta E, \tag{10}$$

where δE represents the discrete term called the shell correction, which can be calculated separately for protons *(Z)* and neutrons *(N),* from the microscopic models. The shell correction term *(δE)* consists of correction due to shape fuctuation *(δE_{sp})* and a correction due to pairing energy *(δE_{pc}),* i.e.,

$$\delta E = \delta E_{sp} + \delta E_{pc}. \tag{11}$$

δE_{sp} can be calculated as the diference between the sum of single-particle energies (ε_i) and their averaged energies [37], given as

$$\delta E_{sp} = E_{sum} - \tilde{E} = \sum_{i=1}^{N_p}\varepsilon_i\left[\sum_{i=1}^{\infty}\varepsilon_i\tilde{n}_i - \gamma_s\tilde{M}_c\right], \tag{12}$$

where N_p is the total number of single particles. The smearing parameter γ_s should be larger than the average energy diference between the two main shells, $\hbar\omega_0 \approx 41A^{-1/3}$. Here $\tilde{n}_i$ are the smoothed occupation numbers, given as

$$\tilde{n}_i = \frac{1}{2}\left[1+\mathrm{erf}(x_i)\right] - \frac{1}{\sqrt{\pi}}\exp\left(-x_i^2\right)\sum_{m=1}^{q}C_m H_{m-1}(x_i), \tag{13}$$

where $x_i = \frac{e-\varepsilon_i}{\gamma_s}$ and erf represents the error function. H_m is the Hermite polynomial with $C_m = \begin{cases} \frac{(-1)^{m/2}}{2^m (m/2)!} & \text{if } m \text{ is even} \\ 0 & \text{if } m \text{ is odd} \end{cases}$ and q is the parameter determining the degree of the polynomial or the order of smearing. $\tilde{M}_c$ is given by

$$\tilde{M}_c = \frac{1}{2\sqrt{\pi}} \sum_{i=1}^{\infty} C_q H_q(\tilde{x}) \exp(-\tilde{x}^2). \tag{14}$$

Where $\tilde{x} = \frac{\tilde{\lambda}-\varepsilon_i}{\gamma_s}$ and $\tilde{\lambda}$ is evaluated using the particle number constraint $\tilde{N}(\tilde{\lambda}) = N_p$, where $\tilde{N}(\varepsilon) = \sum_{i=1}^{\infty} \tilde{n}_i$. The inclusion of $\tilde{M}_c$ makes δE to be less sensitive to γ_s and hence gives a broader plateau for which the conditions are given as

$$\frac{d\tilde{E}}{d\gamma_s} = 0, \qquad \frac{d\tilde{E}}{dq} = 0. \tag{15}$$

The shell correction due to pairing energy (δE_{pc}) is given by [38]

$$\delta E_{pc} = E_{pc} - \tilde{E}_{pc}. \tag{16}$$

E_{pc} and E_{pc} is calculated using the relations

$$E_{pc} = 2\left(\sum_{k=1}^{N_p} \varepsilon_k v_k^2 - \sum_{k=1}^{\frac{N_p}{2}} \varepsilon_k\right) - \frac{\Delta^2}{G} - G\left(\sum_{k=1}^{N_p} v_k^4 - \sum_{k=1}^{\frac{N_p}{2}} 1\right) \text{ and} \tag{17}$$

$$\tilde{E}_{pc} = \frac{-1}{2}\frac{N_p^2}{\tilde{g}(\tilde{\lambda})}\left[\left\{1 + \left(\frac{\tilde{g}(\tilde{\lambda})\tilde{\Delta}}{N_p}\right)^2\right\}^{1/2} - 1\right] + \tilde{g}(\tilde{\lambda})\tilde{\Delta} G \tan^{-1}\frac{N_p}{\tilde{g}(\tilde{\lambda})\tilde{\Delta}}, \tag{18}$$

where $\varepsilon\kappa$ are the single-particle energies calculated using the triaxial Woods-Saxon potential. v_k^2, Δ, and λ are the BCS occupation probability, pairing gap, and chemical potential, respectively. $\tilde{g}(\tilde{\lambda})$ denotes the average level density at the Fermi level which is calculated using

$$\tilde{g}(e) = \frac{1}{\gamma_s\sqrt{\pi}} \sum_{i=1}^{\infty} e^{-x_i^2} \sum_{m=0}^{p} C_m H_m(x_i). \tag{19}$$

$\tilde{\Delta}$ is taken as $\frac{12}{\sqrt{A}}$ in our calculations. The pairing force strength (G) is chosen for protons and neutrons as [39]

$$\begin{aligned} G_p &= \left[g_0^p + g_1^p (N-Z)\right]/A \\ G_n &= \left[g_0^n - g_1^n (N-Z)\right]/A, \end{aligned} \tag{20}$$

where g_0^p, g_1^p, g_0^n, and g_1^n are chosen as 17.90, 0.176, 18.95, and 0.078, respectively.

2.3. The Microscopic Model for GDR

We investigate the infuence of an external time-dependent feld (with energy E)

$$\hat{F}(t) = \hat{F} e^{-i\frac{E}{\hbar}t} + \check{F}\, e^{i\frac{E}{\hbar}t}, \tag{21}$$

where $\hat{F} = \Sigma_{kl} f_{kl}(t) \hat{a}_k \hat{a}_l$ is the one body operator. In quasi-particle picture these operators are transformed into quasi-particle creation ($\beta^\dagger$) and annihilation (β) operators with the restricted canonical Bogoliubov transformation [40] as

$$\beta_m = u_m a_m + \upsilon_m a_m, \tag{22}$$

$$\beta_m = u_m a_m - \upsilon_m a_{\bar{m}}, \tag{23}$$

where v_m^2 is BCS occupation probability of m^{th} quasi-particle state and m refers to the time-reversed conjugation of state m. Any single-particle operator like $\hat{F}$ is transformed to its quasi-particle representation ($\hat{F}$) as [18]

$$\hat{F} = F^0 + \sum_{mm'} F^{11}_{mm'} \beta_m \beta_{m'} + \sum_{m<m'} \left(F^{20}_{mm'} \beta_m \beta_{m'} + F^{02}_{mm'} \beta_{m'} \beta_m\right) \tag{24}$$

where F^0, F^{11}, F^{20} are defned through canonical Bogoliubov transformation [18]. We assume that the feld is weak, i.e., it introduces only linear perturbation in the density matrix of the nucleus. The frst order (linear) change in the density matrix of the nucleus under the infuence of external time-varying perturbation can be written as

$$\rho(t) = \rho_0 + \delta\rho(t), \tag{25}$$

where ρ_o is the density matrix of the unperturbed ground state. The perturbation of the density matrix mirrors the variation of external perturbation over time as

$$\delta\rho(t) = \rho^{(1)} e^{-i\frac{E}{\hbar}t} + \rho^{(1)}\, e^{i\frac{E}{\hbar}t}. \tag{26}$$

Here ρ obeys the following equation of motion

$$i\hbar\dot{\rho} = \left[h(\rho) + f(t), \rho\right], \tag{27}$$

where $h(\rho)$ is the density-dependent single-particle Hamiltonian of the nucleus. $\delta\rho$ is determined by the linear response equation [41, 33, 18]

$$\left(E-E_m+E_{m'}\right)\delta\rho_{mm'}=\left(n_{m'}-n_m\right)\left[F_{mm'}+\frac{1}{2}\sum_{nn'}\upsilon_{mm'nn'}\delta\rho_{nn'}\right], \quad (28)$$

where E_m is the quasi-particle energy of the m^{th} quasi-particle state with its occupation number n_m. $\upsilon_{mm'nn'}$ is the residual interaction that will be treated later as a separable dipole-dipole interaction [Eq. (31)]. We defne the response function (R) through the relation

$$\delta\rho_{mm'}=\frac{1}{2}\sum_{nn'}R_{mm'nn'}(E)F_{nn'}. \quad (29)$$

The response function R is determined by the linearized Bethe-Salpeter equation

$$R=R^0+R^0\cdot\upsilon\cdot R, \quad (30)$$

where R^0 is the response function for vanishing residual interaction. As the form of the perturbation is clearly defned in Eq. (21), our aim is to calculate the response function for a given separable form of residual interaction. We utilize the following separable interaction of the form [41, 33]

$$\hat{H}=\hat{H}_0+\frac{1}{2}\sum_{\alpha=1}^{3}\kappa_\alpha\hat{D}_\alpha\hat{D}_\alpha, \quad (31)$$

where $\hat{H}_0$ is the single-particle Hamiltonian with the WS potential [Eq. (1)]. $\hat{D}_\alpha$ is the single-particle dipole operator and is identical to the external feld operator $\hat{F}$ where α represents the three spatial directions and k_α is the strength parameter of the dipole-dipole force. $\hat{D}_\alpha$ is defined as [42]

$$D_\alpha=\frac{NZ}{A}\left(r^N_{com}-r^P_{com}\right), \quad (32)$$

where r^N_{om} and r^P_{om} are the centers of mass of neutrons and protons, respectively.

The response function represents the change in expectation value of dipole operator $\hat{D}$ in the presence of an external feld of type $\hat{D}$, which oscillates at frequency $\frac{E}{\hbar}$. The response function matrix R can be calculated using the linearized Bethe-Salpeter equation [18, 33, 41], with matrix elements given by

$$R_{\alpha\beta}=\frac{R^0_{\alpha\beta}}{1-R^0_{\alpha\alpha}\kappa_\alpha}, \quad (33)$$

where R^0 is the response function without the residual interaction given by [41]

$$R^0_{\alpha\beta}(E)=\sum_{m<m'}\left(\frac{\langle m'|D^{20}_\alpha|m\rangle\langle m|D^{20^*}_\beta|m'\rangle}{E-E_m-E_{m'}+i\Gamma}-\frac{\langle m'|D^{02}_\beta|m\rangle\langle m|D^{02^*}_\alpha|m'\rangle}{E+E_m+E_{m'}+i\Gamma}\right), \quad (34)$$

where m runs over all the quasi-particle states $(|m\rangle)$. E_m are the quasi-particle energies given by $E_m=\sqrt{(\varepsilon_m-\lambda)^2+\Delta^2}$, where A and Δ are chemical potential and the pairing gap, respectively. ε_m are the single-particle energies that are calculated by diagonalizing the triaxial Woods-Saxon potential [Eq. (9)]. Self consistent values of coupling strengths k_α are [33]

$$\kappa_\alpha=\kappa\frac{3A}{NZ}M\omega^2(\alpha), \quad (35)$$

where $\omega^2(\alpha)$ are the oscillator frequencies corresponding to the structure of the nucleus calculated with the $\hat{H}_0$, and are given by $\hbar(\omega(1)\omega(2)\omega(3))^{\frac{1}{3}}=41A^{\frac{-1}{3}}$ [33]. Here $\omega's$ are inversely proportional tothe semi-axes lengths $R(1)=R(\theta=\frac{\pi}{2},\phi=0)$, $R(2)=R(\theta=\frac{\pi}{2},\theta=\frac{\pi}{2})$, $R(3)=R(\theta=0,\phi=\frac{\pi}{2})$, where $R(\theta,\phi)$ defned through Eq. (3). The resonance peak position is fxed by the parameter κ. The width parameter κ in response function [Eq. (34)] is chosen to be energy dependent [43] as

$$\Gamma_\alpha=\Gamma_0\left(\frac{E_\alpha}{E_0}\right)^\delta, \quad (36)$$

where E_α is the energy of peak in GDR cross-section for spatial direction α and E_0 is the peak energy for zero deformation. Γ_0 is the parameter that determines the width of the cross-section. In this work, the value of δ is taken as 1.9 [5]. The cross-section in the intrinsic frame can be calculated as [33]

$$\sigma(E,\beta_2,\gamma)=\sum_{\alpha=1}^{3}\sigma_\alpha(E,\beta_2,\gamma), \quad (37)$$

where

$$\sigma_\alpha=\frac{-4\pi e^2E}{\hbar c}\mathrm{Im}(R_{\alpha\alpha}), \quad (38)$$

where E is interpreted as the incident energy in the photo-absorption cross-section, and ε is the speed of light in the vacuum.

If the nucleus is rotating with angular frequency ω_{rot} and cranked around the axis of rotation, transforming energies from intrinsic frame to laboratory frame leads to shifting in the energy of amount $\hbar w_{rot}$ and cross-section in lab frame is given as

$$\alpha_{lab}(E,\beta_2,\gamma)=\sum_{\mu=-1}^{1}\sigma\mu(E-\hbar\omega_{rot},\beta_2,\gamma) \quad (39)$$

$$\sigma_\mu=\frac{-4\pi e^2E}{\hbar c}\times\mathrm{Im}\left(R_{D1\mu D1\mu}\right)\left(E-\hbar\omega_{rot},\beta_2,\gamma\right)\Big). \quad (40)$$

The term $R_{D1_\mu D1_\mu}$ is defned as

$$R_{D_{11}D_{11}} = \frac{1}{2}\left(R_{22}+R_{33}\right)+i\left(R_{23}-R_{32}\right) \quad (41)$$

$$R_{D_{10}D_{10}} = R_{11} \quad (42)$$

$$R_{D_{1-1}D_{1-1}} = \frac{1}{12}\left(R_{22}+R_{33}\right)-i\left(R_{23}-R_{32}\right). \quad (43)$$

For a non-rotating nucleus, the cross-section in the lab frame and the intrinsic frame has no diference.

2.4. The Macroscopic Model for GDR

In macroscopic approaches, GDR observables are related to the nuclear shapes irrespective of the details of the mean-feld Hamiltonian or the single-particle states (for more details, see Refs. [44, 11, 10]). In such approaches, we represent the model Hamiltonian $(\hat{H}_M)$ as

$$\hat{H}_M = \hat{H}_{osc} + \eta \hat{D}\ \hat{D}, \quad (44)$$

where $\hat{H}_{osc}$ stands for the anisotropic harmonic oscillator Hamiltonian, η, and $\hat{D}$ are the dipole-dipole interaction strength and dipole operator, respectively. The total GDR cross-section (σ) is the sum of the Lorentzians with peaks at resonance energies (E_α) given by frequencies corresponding to $(\hat{H}_M)$ and can be written as [11]

$$\sigma(E) = \sum_\sigma \frac{\sigma_\alpha}{1+\left(E^2+E_\alpha^2\right)/\left(E^2\Gamma_\alpha^2\right)}, \quad (45)$$

where E is the incident photon energy, σ_α and Γ_α are the peak cross-section and full width at half maximum, respectively. Γ_α is energy dependent as given in Eq. (36) and can be written as [5]

$$\Gamma_\alpha \approx 0.026 E_\alpha^{1.9}, \quad (46)$$

σ_α for component α is given by

$$\sigma_\alpha = 60\frac{2}{\pi}\frac{NZ}{A}\frac{1}{\Gamma_\alpha}0.86(1+\alpha), \quad (47)$$

where a is taken as 0.3. We need not adjust a because it only afects the peak value of the cross-section, and we scale all cross-sections for the sake of comparison within diferent models or experiments.

3. Results and Discussion

We start our discussion by showing our results for the potential energy surface (PES) for the ^{175}Lu which is calculated using the Nilsson-Strutinsky method as discussed in section 2.2. The minimum of the PES corresponds to the most probable shape for the nucleus. In Fig. 1, we show the PES where the black circle represents the minimum. The single-particle energies used in the shell corrections are calculated within the triaxial Woods-Saxon potential. The single-particle wave functions from the same potential are utilized in calculating the GDR response. The equilibrium value of β_2 and γ obtained from the PES is taken as the input for the WS potential used in the GDR response calculations. Our PES show the minimum at the value of $\beta_2 = 0.3$ and $\gamma = 0.0$ which are closer to the finite-range droplet model (FRDM) [45] which gives the value of β_2 as 0.287 whereas the experimental results of E_2 transition probabilities for the neighboring even-even isotope gives the value of β_2 as 0.3226 [46].

Table 1: Comparison of the microscopic model results for centroid energies and the widths of the two humps calculated with different deformation values and the corresponding experimental data [1]. Here E_1 and Γ_1 represent the energy and width of the lower energy peak, and E_2 and Γ_2 are the energy and width of the higher energy peak in the GDR cross-section.

	β_2	E_1 (MeV)	Γ_1 (MeV)	E_2 (MeV)	Γ_2 (MeV)
Exp. [1]	-	12.35	2.70	15.52	4.50
Theory	0.287	12.3	3.9	15.6	4.336
	0.300	12.2	3.0	15.7	4.356
	0.322	12.1	2.8	15.9	4.362

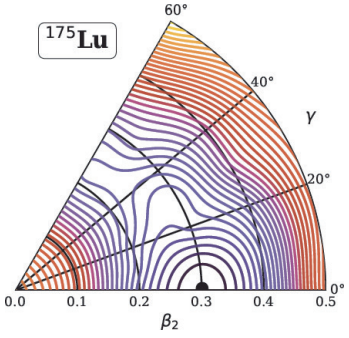

Figure 1: Potential Energy Surface (PES) for ^{175}Lu calculated using triaxial WS potential. The contour line spacing is 0.5 MeV. The minimum is represented with a solid black circle.

After getting the deformation value for the nucleus, we discuss the GDR cross-section results, where we compare the results with the experimental data taken from Ref. [1]. The dipole-dipole interaction strength parameter (κ) is taken as 0.35, and such a reduction in the dipole-dipole interaction strength is necessary to corroborate with the experimental data. [33, 42]. The value of parameter Γ_0 (Eq. (36)) is taken as 1 MeV to match the width of the experimental data. In Fig. 2, we show our results for the GDR cross-section

where we compare the results with the experimental data at three different deformations, i.e., at $\beta_2 = 0.287$ which is obtained from FRDM [45] results [Fig. 2(a)], at $\beta_2 = 0.3$, which is obtained from our PES [Fig. 2(b)], and at $\beta_2 = 0.3226$ taken from Ref. [46] [Fig. 2(c)]. We also compare the experimental results with the results of our macroscopic model, where the value of parameter η is taken as 3.2 [12, 10].

The experimental GDR cross-section shows a two-hump structure as it is a highly deformed prolate nucleus. The microscopic model performs better in reproducing the GDR results in all three cases. However, the macroscopic model is better at reproducing the lower energy hump but overestimates the GDR strength in the higher energy range. On the other hand, the microscopic model fails to reproduce the lower energy hump at deformation given by the FRDM results ($\beta_2 = 0.287$), but when we utilize the higher deformation obtained from our PES ($\beta_2 = 0.3$), the result of the microscopic model starts showing the lower energy hump. This pattern continues when we increase the deformation further using experimental deformation ($\beta_2 = 0.322$). Increasing deformation helps in reproducing the lower energy hump but also contributes to increasing the GDR width. Thus the microscopic results start overestimating the higher energy hump at higher deformation (Fig. 2(c)). The deformation obtained from our PES gives the best fit with the experimental results. This can be understood in terms of the K components as well, where $K = 1$ represents the GDR oscillation along the perpendicular direction to the symmetry axis, which is degenerate as it accounts for two components along the two equal axes, and $K = 0$ shows the component of GDR oscillation along the symmetry axis. For a prolate case like ^{175}Lu, the two components split such that the $K = 0$ component dominates the energy range from 8 to 14 MeV and $K = 1$ branches dominate the 13 to 20 MeV region, which is the cause of the two-hump structure in the microscopic model results. Increasing the deformation leads to increased splitting between these components. Thus, the two-hump structure is enhanced, but this splitting also increases the GDR width, which is reflected in the overall GDR cross-section when we increase the deformation.

In Table 1, we compare the peak energy and widths of the two peaks in the result of the microscopic model with the experimental results from Ref. [1] at all three deformations. The width of the lower energy peak (Γ_1) is better reproduced if we utilize the experimental higher $\beta_2 = 0.322$. Still, the peak positions are better reproduced when we take a lower deformation value from the FRDM. Hence, the intermediate deformation provided by our PES provides the best fit with the experimental data. We have established that the microscopic model can reproduce the GDR results in an odd nucleus like ^{175}Lu, giving a better result than the macroscopic model. The deformation obtained from our PES value of deformation gives the best fit with the experimental data.

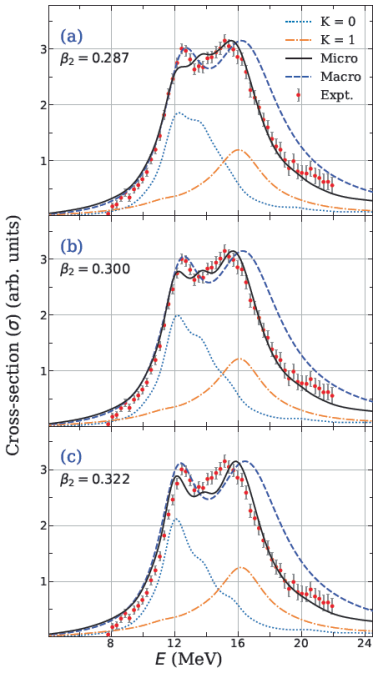

Figure 2: Experimental GDR cross-sections of ^{144}Nd (filled-circles) taken from Ref. [1] are compared with the microscopic (solid line) and macroscopic (dashed line) model calculations with deformations obtained from: (a) the finite-range droplet model (FRDM) [45], (b) our PES from Fig. 1, and (c) the experimental results of $E'l$ transition probabilities for the neighboring even-even isotope [46]. The corresponding contribution of $K = 0$ and $K = 1$ components is also shown.

4. Conclusions

In the present work, we have presented a microscopic model for GDR based on the linear response theory. The underlying single-particle structure is obtained using the triaxial Woods-Saxon (WS) potential. We have investigated the isovector GDR in ^{175}Lu which is a highly deformed prolate nucleus. The deformation of the nucleus is obtained within the microscopic-macroscopic approach of the Nilsson-Strutinsky method. The same WS potential used in the linear response theory is used for obtaining the shell corrections. We also compare our results with the results of the macroscopic model to establish a benchmark.

Our results show that the microscopic model performs better than the macroscopic model, especially in the higher energy region; however, the macroscopic model better

reproduces the lower energy hump in the experimental data. We also compare the results at three different deformations, including the deformation obtained from the finite range droplet model results and the results of E_2 transition probabilities of the neighboring even-even isotope, and the equilibrium deformation obtained from our microscopic macroscopic approach.

Our results show that the overall best ft with the experiment is obtained with the deformation given by our potential energy surface. This corrobora-tion favors the self-consistent approach as both the PES and the microscopic model depend upon the same mean feld of the triaxial WS potential. The GDR strength for a prolate nucleus is split into the $K = 0$ and $K = 1$ branches, and the microscopic model reasonably reproduces a two-hump structure. The extension of this microscopic model to a thermally excited system can prove helpful as most of the macroscopic model is already very successful in such regimes, and only a few microscopic studies are done in hot and rotating nuclei.

Authorship Contribution

Abhishek: has done all the calculations and analysis of the results in the present work.

Confict of Interest

The author has no confict of interest.

Declaration

The present work has not been published elsewhere and is not sent elsewhere journal.

References

[1] R. Bergère et al. Nuclear Physics A 1**33**, 417– 437. https://www.sciencedirect.com/science/article/pii/0375947469906447.

[2] M. N. Harakeh and A. Van derWoude. Giant Resonances: Fundamental High-Frequency Modes of Nuclear Excitation. Oxford University Press, Oxford, 2001.

[3] W. Bothe and W. Gentner. Z. Phys. **106**, 358–361. https://doi.org/10.1007/BF01338744.

[4] B. L. Berman and S. C. Fultz. Rev. Mod. Phys. **47**, 713–761. https://link.aps.org/doi/10.1103/RevModPhys.47.713.

[5] P. Carlos et al. Nucl. Phys. A **219**, 61. https: //doi.org/10.1016/0375-9474(74)90082-7.

[6] L.M. Donaldson et al. Phys. Lett. B **776**, 133. https://doi.org/10.1016/j.physletb. 2017.11.025.

[7] Mukul, Ish et al. EPJ Web Conf. **63**, 01020. https ://doi.org/10.1051/epjconf/20136301020.

[8] C. Ghosh et al. Phys. Rev. C **94**, 014318. https://link.aps.org/doi/10.1103/PhysRevC.94.014318.

[9] K Goeke and J Speth. Annu. Rev. Nucl. Part. Sci. **32**, 65–115. https://doi.org/10.1146/annurev.ns.32.120182.000433.

[10] A. K. Rhine Kumar and P. Arumugam. Phys. Rev. C **92**, 044314. https://link.aps.org/doi/10.1103/PhysRevC.92.044314.

[11] P. Arumugam, G. Shanmugam, and S. K. Patra. Phys. Rev. C **69**, 054313. https://link.aps.org/doi/10.1103/PhysRevC.69. 054313.

[12] P. Arumugam, A. Ganga Deb, and S. K. Patra. Eur. Phys. J. A **25**, 199. https:// doi.org/10.1140/epja/i2005-10080-8.

[13] J. A. Maruhn et al. Phys. Rev. C **71**, 064328. https://link.aps.org/doi/10.1103/PhysRevC.71.064328.

[14] Kenichi Yoshida and Takashi Nakatsukasa. Phys. Rev. C **83**, 021304(R). https://link.aps.org/doi/10.1103/PhysRevC.83.021304.

[15] A. Ait Ben Mennana and Mostafa Oulne. Eur. Phys. J. Plus **136**, 85. https://doi.org/10.1140/epjp/s13360-020-01017-z.

[16] Y. Alhassid. Nucl. Phys. A **649**, 107–114. https://www.sciencedirect.com/science/article/pii/S0375947499000470.

[17] W. E. Ormand, P. F. Bortignon, and R. A. Broglia. Phys. Rev. Lett. **77**, 607–610. https://link.aps.org/doi/10.1103/PhysRevLett.77.607.

[18] P. Ring and P. Schuck. The Nuclear Many-Body Problem. Springer, 2004. https://books.google.co.in/books?id=PTynSMnMA8C.

[19] Nguyen Dinh Dang and Akito Arima. Phys. Rev. Lett. **80**, 4145–4148. https://link.aps.org/doi/10.1103/PhysRevLett.80. 4145.

[20] W. Kleinig et al. Phys. Rev. C **78**, 044313. https://link.aps.org/doi/10.1103/PhysRevC.78.044313.

[21] S. S. Wang et al. Phys. Rev. C **95**, 054615. https://link.aps.org/doi/10.1103/PhysRevC.95.054615.

[22] Tomohiro Oishi, Markus Kortelainen, and Nobuo Hinohara. Phys. Rev. C **93**, 034329. https://link.aps.org/doi/10.1103/PhysRevC.93.034329.

[23] N. Paar et al. Phys. Rev. C **67**, 034312. https://link.aps.org/doi/10.1103/PhysRevC.67.034312.

[24] T. Nikšić, D. Vretenar, and P. Ring. Phys. Rev. C **66**, 064302. https://link.aps.org/doi/10.1103/PhysRevC.66.064302.

[25] Y. Alhassid and B. Bush. Phys. Rev. Lett. **63**, 2452–2455. https://link.aps.org/doi/10.1103/PhysRevLett.63.2452.

[26] S.K. Patra et al. Nucl. Phys. A **703**, 240– 268. https://www.sciencedirect.com/science/article/pii/S0375947401015317.

[27] B.K. Agrawal, A. Ansari, and P. Ring. Nucl. Phys. A **615**, 183–197. https://www.sciencedirect.com/science/article/pii/S0375947497000122.

[28] Ahmad Ansari, Nguyen Dinh Dang, and Akito Arima. Phys. Rev. C **62**, 011302(R). https://link.aps.org/doi/10.1103/PhysRevC.62.011302.

[29] Ahmad Ansari, Nguyen Dinh Dang, and Akito Arima. Phys. Rev. C **63**, 024310. https://link.aps.org/doi/10.1103/PhysRevC.63.024310.

[30] G. Noguere et al. Phys. Rev. C **100**, 065806. https://link.aps.org/doi/10.1103/PhysRevC.100.065806.

[31] E. Tabar et al. European Physical Journal A **58**, 101, 101. https://ui.adsabs.harvard.edu/abs/2022EPJA...58..101T.

[32] Emre Tabar et al. Nuclear Physics A **1001**, 121885. https://doi.org/10.1016/j.nuclphysa.2020.121885.

[33] M. Isabel Gallardo et al. Nucl. Phys. A **443**, 415. https://doi.org/10.1016/0375-9474(85)90409-9.

[34] Jerzy Dudek et al. Phys. Rev. C **26**, 1712– 1718. https://link .aps.org/doi/10.1103/PhysRevC.26.1712.

[35] V.M. Strutinsky. Nucl. Phys. A **95**, 420– 442. https://www.sciencedirect.com/science/article/pii/0375947467905106.

[36] V. M. Strutinsky. Nucl. Phys. A **122**, 1– 33. https://www.sciencedirect.com/science/article/pii/0375947468906994.

[37] O. Civitarese, A. L. De Paoli, and A. Plastino. Z. Phys., A At. nucl. **309**, 177–181. https: //doi.org/10.1007/BF01414979.

[38] M. Bolsterli et al. Phys. Rev. C **5**, 1050–1077. https://link.aps.org/doi/10.1103/PhysRevC.5.1050.

[39] J Dudek, A Majhofer, and J Skalski. J. Phys. G: Nucl. Part. Phys. **6**, 447–454. https://doi.org/10.1088/0305-4616/6/4/013.

[40] M. Brack and P. Quentin. Nuclear Physics A **361**, 35–82.

[41] P. Ring et al. Nucl. Phys. A **419**, 261. https://doi.org/10.1016/0375-9474(84)90393-2.

[42] P. Ring and J. L. Egido. Prog. Part. Nucl. Phys. **9**, 449. https://doi.org/10.1016/0146-6410(83)90026-1.

[43] Michael Danos and Walter Greiner. Phys. Rev. **134**, B284–B296. https://link.aps.org/doi/10.1103/PhysRev.134.B284.

[44] G. Shanmugam and M. Thiagasundaram. Phys. Rev. C **37**, 853–859. https://link.aps.org/doi/10.1103/PhysRevC.37.853.

[45] P. M̈oller et al. At. Data Nucl. Data Tables **109**, 1–204. http://inis.iaea.org/search/search.aspx?orig_q=RN:51081571.

[46] B. Pritychenko et al. At. Data Nucl. Data Tables **107**, 1–139. https://www.sciencedirect.com/science/article/pii/S0092640X15000406.

Journal of Nuclear Physics, Material Sciences, Radiation and Applications

Chitkara University, Saraswati Kendra, SCO 160-161, Sector 9-C, Chandigarh, 160009, India

Volume 10, Issue 1 **August 2022** **ISSN 2321-8649**